RSC Advances

PAPER

View Article Online
View Journal | View Issue

Cite this: *RSC Adv.*, 2024, **14**, 28455

Nanostructured layered double hydroxide (NLDH) – Zn/Al-based materials: strategy to improve performance for zirconium sorption from acidic sulfate solution†

Ahmed M. Masoud, [a] Amal E. Mubark, *[a] Mohamed H. Taha [a] and Saber Ibrahim [bc]

Zirconium is a highly stable radionuclide commonly used in various nuclear operations. However, removing zirconium from wastewater streams is crucial to protect the environment and human health. To achieve this, a zinc and aluminum nanostructured layered double hydroxide (Zn/Al-NLDH) was prepared and investigated for effective removal of zirconium from aqueous solutions. This study examined the prepared Zn/Al-NLDH's structural and textural properties and the impact of various factors on its adsorption performance. The Langmuir isotherm and Pseudo-second order kinetic models were found to be the best fit for the adsorption process of Zr(IV). This suggests that the adsorption process is uniform, involves the formation of a monolayer, and is chemisorption in nature. The maximum uptake capacity was 117.6 mg g^{-1}, and the process was endothermic, spontaneous, and feasible. About 96% of Zr(IV) was successfully desorbed from the loaded sorbent using 1.0 M hydrochloric acid, and the Zn/Al-NLDH sorbent remained stable for six consecutive sorption/desorption cycles. These findings emphasize the high potential of Zn/Al-NLDH to act as a remarkable sorbent for efficiently tackling water contaminants.

Received 24th May 2024
Accepted 1st September 2024

DOI: 10.1039/d4ra03845b

rsc.li/rsc-advances

1 Introduction

Zirconium and its alloys are highly valuable for the nuclear industry. They are used as coating materials for fuel pellets and nuclear reactors due to their low thermal neutron capture cross-section and high melting point.[1–5] In the chemical industry, zirconium/nickel alloys are used to obtain materials resistant to corrosion[6] while superconducting magnets can be made with zirconium/niobium alloys due to their superconductivity at low temperatures.[7] Moreover, zirconium oxide with lower purity is used in the ceramics industry.

Methods and highly selective extractants for the recovery of zirconium have recently become crucial due to the rising demand for the manufacturing of high-grade zirconium and its compounds and also for purifying wastewater to obtain pure water which could be used for further application. Traditional techniques such as ion exchange,[7,8] solvent extraction,[9,10] fractional crystallization,[11] and fractional precipitation[12] are frequently utilized. Extractants such as methyl isobutyl ketone (MIBK), N235, and TBP are used in solvent extraction.[10] The recovery of metal ions using ion exchange in industry is typically done on a fixed bed. The Zr retrieval has been carried out using extractant-impregnated resin as well as cation- and anion-exchange resins.[13,14] In the case of ion exchange, different anion and cation ion exchangers are used. Strong-base anion exchange resins are the most popular, and zirconium is adsorbed from concentrated hydrochloric acid or diluted sulfuric acid solutions instead of hafnium.[14,15] Nevertheless, industrialization of these approaches is constrained due to their drawbacks of high treatment capacities, high efficiency, and environmental pollution.[16–19] There is an urgent need for the development of extremely effective techniques for the removal of zirconium utilizing highly precise ion identification extractants.

The adsorption process provides viable alternatives for the recovery of metal ions from aqueous effluents owing to its cost and energy efficiency, insensitivity to toxic pollutants, and design simplicity and flexibility.[2,6,18,19] Separating metals from these effluents is a highly challenging task due to their complex composition. The features of the adsorbent have a significant impact on the effectiveness of adsorption. Layered double hydroxide (LDH) is a layered substance made up of layers of divalent and trivalent metal ions with anion spaces in between.[20–22] Depending on the synthetic conditions and application goals, the anion on the interlayer space may be

[a]*Nuclear Materials Authority, P. O. Box 530, El Maddi, Cairo, Egypt*
[b]*Packaging Materials Department, National Research Centre, 12622, Dokki, Cairo, Egypt. E-mail: amal_mubark2014@yahoo.com; Tel: +201018600164*
[c]*Nanomaterials Investigation Laboratory, Central Laboratories Network, National Research Centre, Dokki, Cairo, 12622, Egypt*

† Electronic supplementary information (ESI) available. See DOI: https://doi.org/10.1039/d4ra03845b

interchangeable. Sulfate, carbonate, hydroxide, nitrate, chloride, and large-sized anion such as polyoxometalate are the most prevalent cations on interlayer LDH.[20–22] The typical formula for LDH is $[M_{1-x}^{2+}M_x^{3+}(OH)_2] + xA_{x-n}\cdot mH_2O$, where M^{2+} and M^{3+} are divalent and trivalent metal ions, respectively, A_{x-n} is an anion with n oxidation state or valence, and m is the crystallization water.[23,24] The LDH has a large surface area and a high adsorption capacity, making it a popular adsorbent. The modification of LDH is an intriguing topic in the search for a stable adsorbent, however, as LDH is generally unstable when used as a material for several adsorption processes.[23,24] The presence of LDH in the form of nanomaterial enhances its characteristic behaviors towards the adsorption of heavy metal ions with proper stability.

An effort has been made in the current study to modify the LDH material to produce nanostructured layered double hydroxide (NLDH), a Zn/Al-based material that will be used as an adsorbent for Zr(IV) ions. NLDH was characterized based on physical and chemical methods such as XRD, TEM, BET surface area, and particle size analysis. Elution, as well as selectivity tests, were also performed. The impact of various factors affecting the sorption process of Zr(IV) ions has been investigated. The outcomes of this study will also be contrasted with previously published data on the sorbent's performance of chelating resins. Thermodynamic and kinetic parameters were estimated. The prepared (NLDH) Zn/Al-based material nanomaterial was evaluated on lab waste effluent collected from Nuclear Materials Authority labs.

2 Materials and methods

2.1. Materials

The consumed chemicals during this study were of analytical grade and applied as supplied. Sodium dodecyl sulfate (SDS), aluminum nitrate nonahydrate, zinc acetate dihydrate, sodium hydroxide, and sodium nitrate were bought from Sigma-Aldrich (Sigma-Aldrich Company Ltd, Poole, Dorset, UK). Deionized water was employed for the preparation of all aqueous solutions. Zirconyl oxychloride ($ZrOCl_2\cdot 8H_2O$; 99.9%) salt was used to prepare 1.0 g L^{-1} of Zr(IV) ions stock solution. Aluminum nitrate nonahydrate ($Al(NO_3)_3\cdot 9H_2O$; 99.9%), and zinc acetate dihydrate ($C_4H_6O_4Zn\cdot 2H_2O$; 99.9%) were purchased from Sigma-Aldrich Chemical Co, USA, and utilized for the sorbent synthesis process. Fresh-prepared Zr(IV) standard solutions were synthesized from the stock solution.

2.2. Synthesis of NLDH-Zn/Al sorbent

Zinc–aluminum layered double hydroxide (Zn/Al-NLDH) with a stoichiometric ratio was prepared under nitrogen gas to avoid carbonation. This was done by dissolving zinc acetate dihydrate and aluminum nitrate nonahydrate in decarbonated distilled water. The resulting solution was then added dropwise to another solution containing 25 g of sodium hydroxide and 20 g of sodium nitrate. The mixture was stirred forcefully at 65 °C for 5 hours. The pH of the dispersion was adjusted to 8.5 using a 0.1 M NaOH solution. After maturing for 5 days, the deposit was centrifuged, washed once with decarbonated distilled water, and re-centrifuged. The final product was dried at 85 °C.

2.3. Sorbent characterization

Dynamic light scattering (DLS) was used to determine the mean diameter of the synthesized Zn/Al-NLDH particle using NICOMP 380 (ZLS, PSS Santa Barbara, CA, USA). The distribution of particle diameter was measured according to scattering laser light through more than 700 incident times. The intensity Gaussian distributions were collected as a mean of multiple measurements and calculated by the average particle diameter. BET surface area was calculated from nitrogen adsorption–desorption measurements using Nova Touch LX4 (Quantachrome, USA). The conditions of measurements of particle size and surface area were described in previous work.[25] The powder Zn/Al-NLDH was characterized using XRD (D8 Advance, Bruker AXS) with CuKα radiation (λ of 1.5406 Å). LDH was prepared by dropping a solution on a carbon-coated copper grid (S160-3 Plano GmbH) and investigated using a JEOL 120/JEOL 200 TEM (Carl Zeiss NTS) operated at 120 kV/200 kV. The morphology of the composite surface was examined using a scanning electron microscope (SEM), specifically a QUANTA FEG 250 model from the USA, with an accelerating voltage of 30 kV and a magnification range of 14 to 1 000 000 times. This microscope has a high resolution of 1 nm and is equipped with an energetic dispersive X-ray (EDX) unit to facilitate quantitative elemental analysis of specimens. Fourier-transform infrared spectroscopy (FTIR) was used to analyze the samples. A PerkinElmer Spectrometer 400 equipped with a Golden Gate diamond single reflection device was used for this purpose.

2.4. Adsorption experiments

The study aimed to determine the effectiveness of Zn/Al-NLDH material in adsorbing Zr(IV) ions. The experiments were conducted in polypropylene tubes with a definite weight of Zn/Al-NLDH material (m, g) and a specific volume of aqueous phase (V, L). The materials were combined for a set time (t, min) using a SWB 27–27 L thermo-shaker water bath. The initial concentration of Zr(IV) was (C_o; 50 mg L^{-1}), and the pH of the solution was monitored using a Cyber Scan pH 6000 pH-meter (Eutech Instruments, Netherlands), which was maintained using 0.5 M HCl and 0.5 M NaOH. After the required shaking time, the solution was filtered using a 1.2 μm filter membrane. The concentration of Zirconium in the aqueous phase (C_e, mg L^{-1}) was measured using ICP-AES (inductively-coupled plasma atomic emission spectrometer, Activa M, Horiba-Jobin Yvon, France). The tests were repeated thrice, and only a ≤4% standard error value was presented. Eqn (1)–(3) were used to calculate the Zn/Al-NLDH's adsorption capacity (q_e, mg g^{-1}), removal efficiency (%), and distribution coefficient (K_d, mL g^{-1}).

$$q_e = (C_o - C_e) \times \frac{V}{m} \quad (1)$$

$$\% = \frac{C_o - C_e}{C_o} \times 100 \quad (2)$$

$$K_d = \frac{(C_o - C_e)}{C_e} \times \frac{V}{m} \quad (3)$$

3 Results and discussion

3.1. Sorbent characteristics

3.1.1. Particle size and zeta potential. Particle size is one of the unique characteristics of dispersed NLDH. Laser Light Scattering involves shining a laser beam on the particles. As the laser light hits the particles, it scatters in different directions. The distribution of particle diameter was measured according to the scattering laser light technique through more than 700 collisions times.[26] The number of collisions times refers to the number of measurements or interactions between the laser light and the particles. Each "collision" helps gather data on how the light is scattered, which is used to calculate the size distribution of the particles. The intensity Gaussian distributions were collected as a mean of multiple measurements and calculated the average particle diameter for Zn/Al-NLDH. The bell shape distributions were illustrated in Fig. 1 for Zn/Al-NLDH before and after treatment. The mean of particle distribution was varied according to Zn/Al-NLDH ≈140 nm and increased to 268 nm after treatment. Well-defined homogenized distribution is presented with a regular distribution width. This is confirmed by the polydispersity index (PDI) which indicated 0.08 and 0.61 for NLDH and Zr-NLDH, respectively.

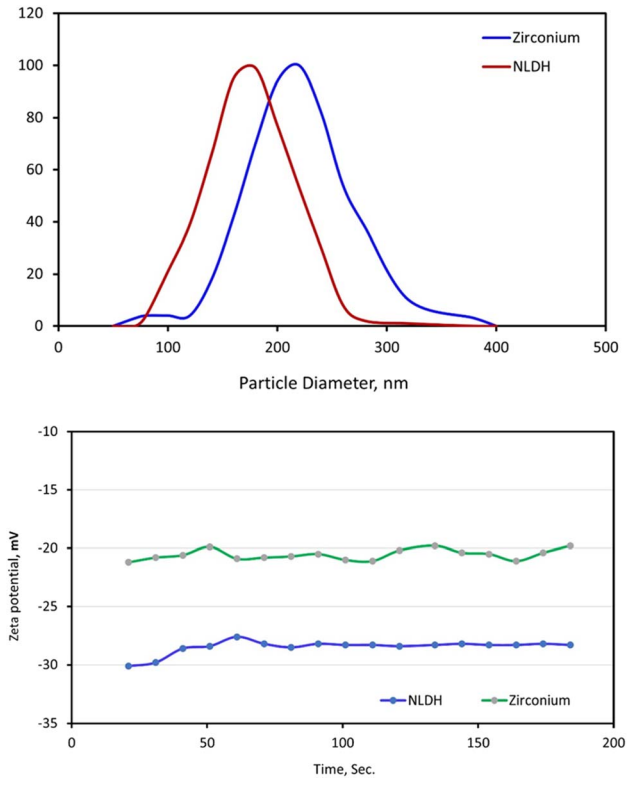

Fig. 1 (I) Particle size distribution and (II) zeta potential of the prepared Zn/Al-NLDH before and after adsorption.

On the other hand, the zeta potential of mobilized particles in aqueous medium through collisions and Brownian motion was measured. The charge of NLDH was indicated by −28.9 mV whereas the zeta charge after treatment with Zr(IV) ≈ −19.8 mV. This phenomenon could be related to the electrostatic interaction of zirconium cation with a negative charge of hydroxide layers in NLDH that decreases the charge by 32%.

3.1.2. X-ray diffraction. XRD pattern of Zn/Al-NLDH prepared using a high concentration of base solution. The obtained Zn/Al-NLDH and Zn/Al-mixed oxide structures show significant crystal form are compared to other indices which could be promising in applications to heavy metals sorption. Fig. 2 presents the XRD patterns of Zn/Al-NLDH. As is shown, the characteristic reflections of basal peaks in the range of 2θ = 31.715–68.972° were expanded which indicated a degree of exfoliation for NLDH layers. Therefore, a good dispersion is observed which means there is an intercalation between Zn/Al-NLDH nanomaterial. The average crystallite size of Zn/Al-NLDH was calculated by the Scherrer equation eqn (4):[2]

$$D = K\lambda/h_{1/2}\cos\theta \quad (4)$$

Where D is the average crystallite size, K is the Scherrer constant (0.9), λ is the wavelength of the X-ray radiation (0.1541 nm for CuKα), $h_{1/2}$ was the peak width at half height and θ corresponded to the peak position. The average crystallite size of the Zn/Al-NLDH is 3 nm.

3.1.3. Surface area. The occupied area by an object in three dimensions through its outer surface is called the surface area. There are two main types of surface area: the outer surface area and inner surface area by pore size of hollow materials.[27] The surface area of NLDH before and after Zr(IV) treatment was tabulated in Table 1. The reduction in the surface area after treatment could be related to the aggregation of surface-charged particles with zirconium ions.

3.1.4. TEM investigation. The morphological structure of NLDH before and after treatment with Zr(IV) waste sample was presented in Fig. 3. The particle form of NLDH was presented in the image (A) as semi-individual inorganic particles with a range from 17 nm up to 50 nm. In addition, image (B) illustrated the aggregation form of NLDH-Zr after treatment with particle sizes 49 to 73 nm. The crystal pattern of NLDH before and after treatment with Zr(IV) presented identified rings.

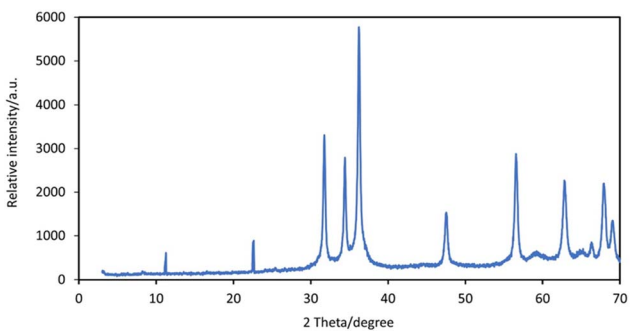

Fig. 2 X-ray diffraction of the prepared NLDH.

Table 1 Surface area of the prepared NLDH in adsorption isotherm branch

Sample	Isotherm branch	Slop	Intercept	Correlation coeff. (R)	Surface area ($cm^2\ g^{-1}$)	Pore volume $10^{-1}\ cm^3\ g^{-1}$
NLDH	Adsorption	4.86	−0.095	0.996	730.5	4.15
Zr-NLDH		20.68	0.641	0.999	163.3	5.43

3.1.5. SEM characterization. Fig. 4 depicts the morphological structure of the analyzed zirconium composites as seen by field emission scanning electron microscopy. The predicted findings in Fig. 4 show that NLDH and NLDH-Zr have markedly different surface shapes, with differing degrees of porosity, roughness, and pore structure. The NLDH adsorbent was composed of semi-uniformly sized particles with varied shapes. The presence of bumps and fissures between adsorbent granules facilitated adsorption and rapid solution diffusion. The surface roughness of NLDH-Zr seems rougher than that of NLDH, which aids in the adsorption of zirconium ions on the NLDH.

As a consequence of the preparation indicated in Fig. 4, the adsorbent was predominantly composed of carbon (C), oxygen (O), zinc (Zn), and aluminum (Al), which matched the expected prepared adsorbent (NLDH). According to the EDX measurement before and after the adsorption procedure, the elemental compositions alter due to Zr(IV) adsorption on the surface of NLDH. The EDX analysis of NLDH-Zr (Fig. 4) shows that it has a similar elemental composition to NLDH, with the presence of zirconium (Zr) and sulfur (S) peaks that contribute to metal ion adsorption in the acidic medium (sulfate). This demonstrates the effective attachment of zirconium from the sulfate medium *via* the prepared NLDH.

3.1.6. FTIR investigation. FT-IR spectroscopy is a fundamental approach for chemical investigation, monitoring the functional groups and various bonds of the examined compounds, and predicting their structure. Fig. 5 depicts the FT-IR charts of NLDH in its initial and loaded forms. The broad band at 3448 cm^{-1} is related to the stretching of the OH bond (it is a transverse package as it is a combination of vibrations from different types of hydroxyl groups present in the sample. These

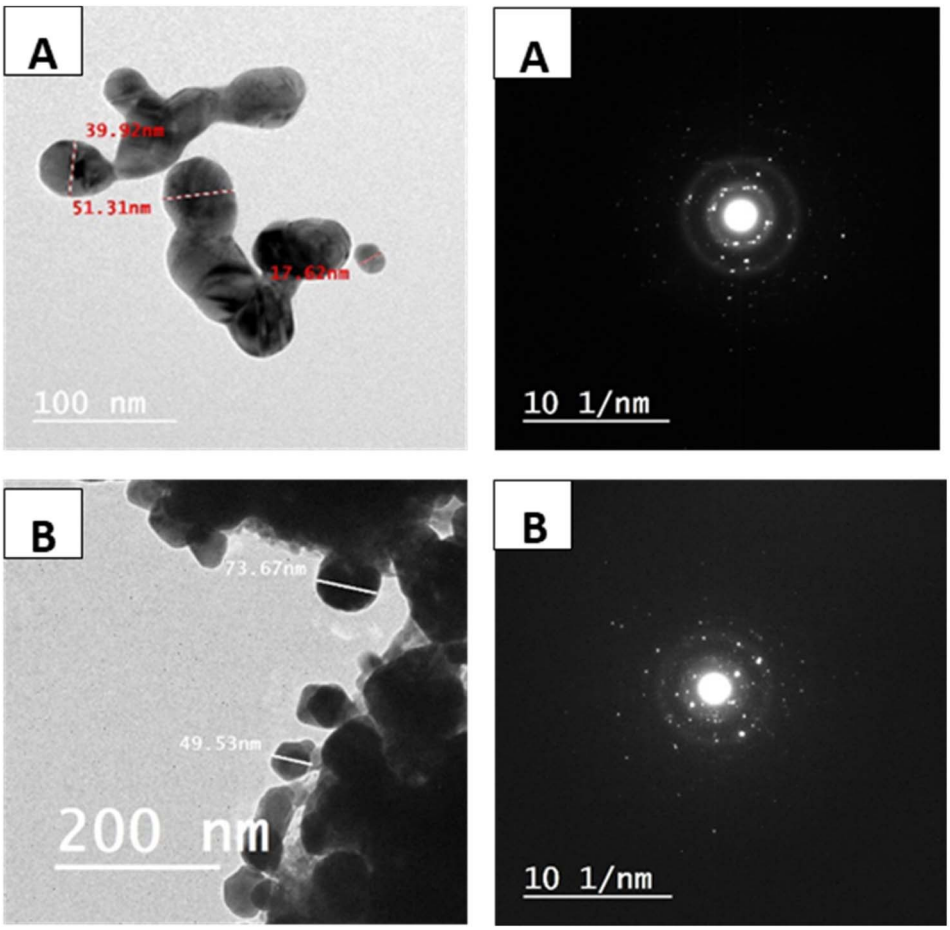

Fig. 3 TEM topography of the prepared NLDH before adsorption (A) and after loading with Zr(IV) ions (B).

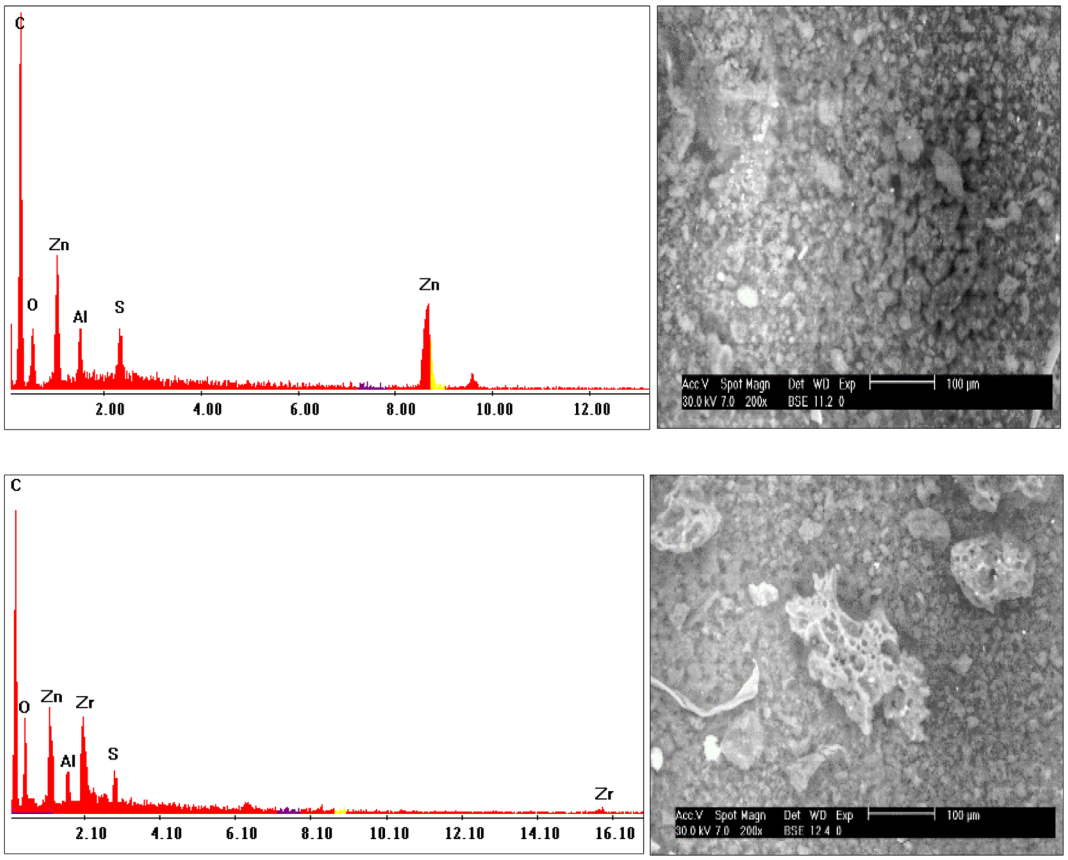

Fig. 4 SEM-EDX of NLDH before and after Zr(IV) adsorption.

could include hydroxyl groups associated with the layered structure of Zn/Al-NLDH and hydroxyl groups from physically adsorbed water).[28,29] The weak band at 1731 cm^{-1} corresponds to the bending vibration of interlayer water. The bands at 460, 669, and 751 cm^{-1} correspond to Al–O condensed groups, Zn/Al–OH translation, and Al–OH deformation, respectively.[30] The adsorption of zirconium ions produces several different changes. Zr(IV) ions interact with NLDH active sites, resulting in a band at 2360 cm^{-1}. Aside from this new peak, there were changes in certain bands that demonstrated the efficacy of the adsorption of Zr(IV) ions on NLDH adsorbent.

3.2. Process of Zr(IV) adsorption

3.2.1. Impact of solution pH. The pH of a solution plays a crucial role in adsorption systems. It determines the adsorbate species and the surface charge of the sorbent in the aqueous solutions. The insoluble Zr(IV) ion species ($Zr(OH)_4$) predominates at pH levels higher than 2.0,[2,6] so the impact of the solution pH range (1.0–2.0) on the Zr(IV) adsorption using Zn/Al-NLDH sorbent was investigated by conducting a set of tests at a fixed 0.5 g L^{-1} sorbent dosage, 120 min shaking time of, 50 mg L^{-1} original concentration, and room temperature. The results in Fig. 6 revealed that the sorption capacity boost from 13.3 to 90.6 mg g^{-1} with the solution pH increment from 1.0 to 2.0 respectively. Further increasing the solution pH had a slight impact on the adsorption capacity.

The behavior of Zr(IV) ions in solution at varying pH levels, and the analysis of zeta potential for the sorbent used can explain the performance of Zn/Al-NLDH sorbent at different pH levels. Fig. 1 explores that Zn/Al-NLDH possesses a negatively charged surface (−28.9 mV). Furthermore, Zr(VI) ions exist as cationic species such as $Zr_4(OH)_8^{8+}$, $ZrOH^{3+}$, and $Zr_3(OH)_5^{7+}$ at a pH of ≤2,[2–4] which have a strong tendency to bind to negatively charged sorbent surfaces. However, at low pH levels, there is high competition between hydrogen ions and Zr(IV) cationic species for binding with the Zn/Al-NLDH sorbent surface functional groups, which negatively affects the sorption capacity.[2–4] By increasing the pH of the solution, the concentration of H^+ decreases, giving more opportunities for Zr(IV) cations to interact with the sorbent's active sites.[2–4] However, extending the solution to pH > 2.0, the insoluble Zr(IV) species (ZrO_2) becomes the predominant species, resulting in a decrease in adsorption affinity. The similar sorption performance was elucidated for Zr(IV) adsorption from aqueous solution by magnetic cellulose/chitosan nanocomposites,[2] *in situ*-gel-precipitated aluminum-based composite sorbents modified,[3] polyacrylamide titanium tungstosilicate,[6] polyaniline/SiO_2 composite,[16,17] activated charcoal,[31] and clinoptilolite.[32]

3.2.2. Kinetic investigation. The adsorption mechanism and system scaling up can be observed by analyzing the data generated from the adsorption kinetic analysis. The adsorption

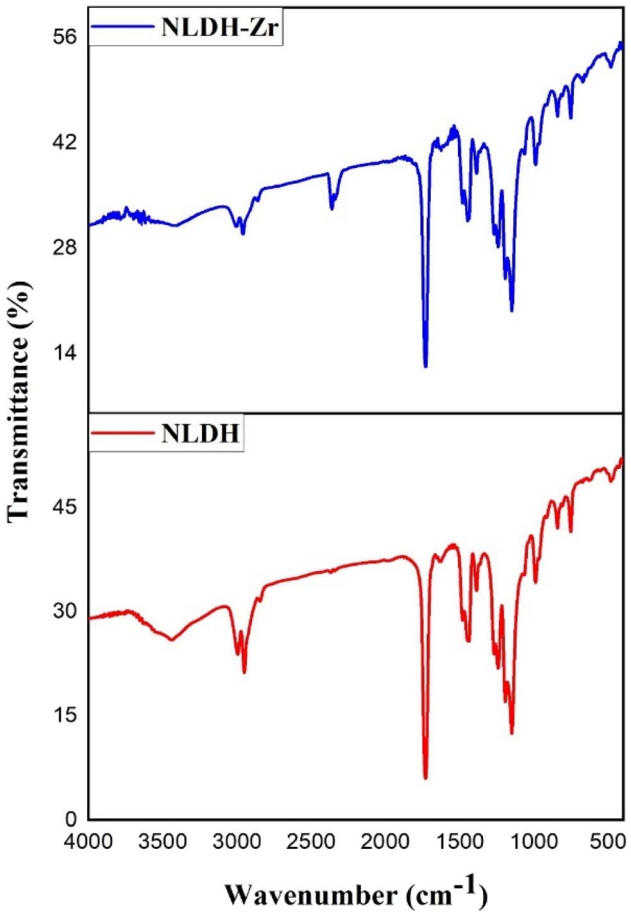

Fig. 5 FTIR of NLDH before and after Zr(IV) adsorption.

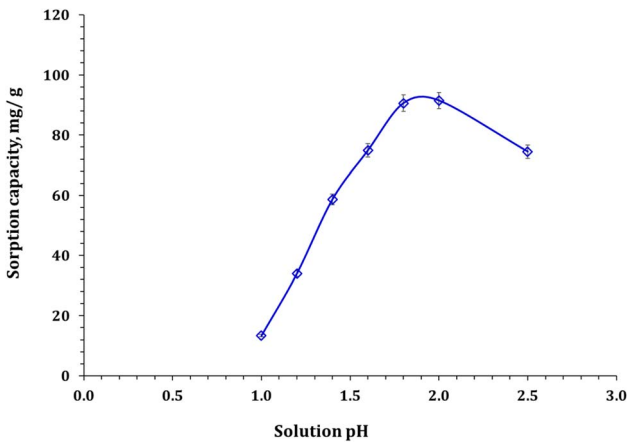

Fig. 6 Zr(IV) sorption capacity as a function of solution pH (mixing time: 120 min; room temperature; Zr(IV) initial concentration: 50 mg L^{-1}; and sorbent dose: 0.5 g L^{-1}).

tendency of Zn/Al-NLDH was examined over different time intervals ranging from 5 to 240 minutes, using a fixed sorbent dose of 0.5 g L^{-1}, a pH of 2.0, a temperature of 25 ± 1 °C, and 50 mg L^{-1} an original concentration of. Fig. 7 shows a significant increase in sorption affinity until the equilibrium time of

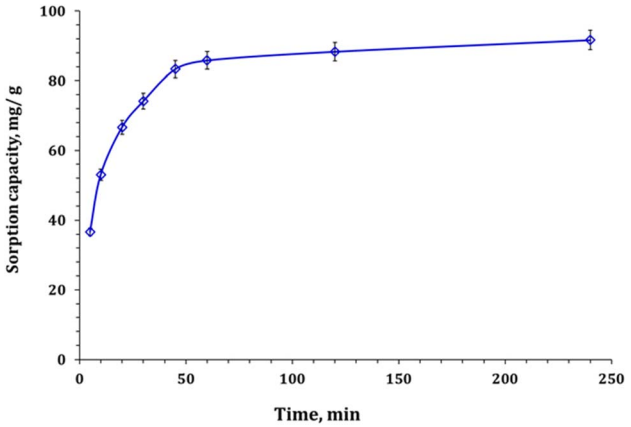

Fig. 7 Zr(IV) sorption capacity as a function of time (pH: 2.0; room temperature; Zr(IV) initial concentration: 50 mg L^{-1}; and sorbent dose: 0.5 g L^{-1}).

45 minutes, with a sorption capacity of about 83.3 mg g^{-1}. After the equilibrium time, the sorption affinity levels off. This behavior is attributed to the accessibility of vacant function groups on the surface of the Zn/Al-NLDH sorbent before equilibrium time. Most of these active sites were occupied with Zr(VI) ions beyond equilibrium time.[16,17]

Zr(VI) adsorption kinetic using Zn/Al-NLDH material can be analyzed by studying the results obtained from Weber–Morris, Lagergren, and Pseudo-second-order models.[33–36] The main concept of each model is explained in the corresponding references. The nonlinear equations for each model are given in Table S1.†[28–31] The fitting of the models is determined using the Chi-square (χ^2) and correlation coefficient (R^2) equations (Table S1†). The sorption capacity *vs.* shaking time plot is shown in Fig. 8 and the values of the kinetic terms are presented in Table 2. Based on the investigated data, it has been determined that the Pseudo-second-order kinetic model provides the best description for the experimental results. This model has the lowest Chi-square coefficient (χ^2: 0.16) and the highest coordination coefficient (R^2: 0.99). This indicates that the rate-

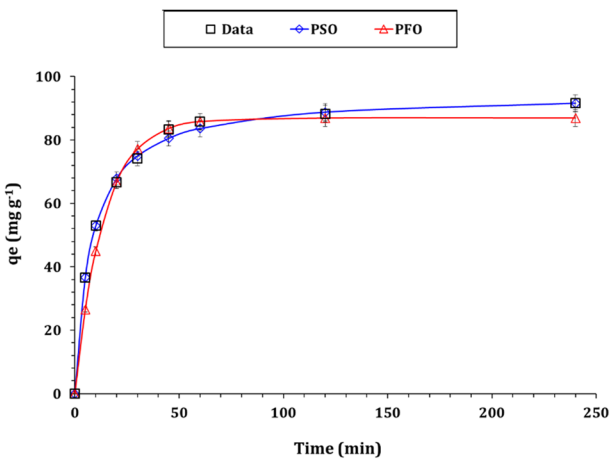

Fig. 8 The kinetic curve of Zr(IV) sorption using Zn/Al-NLDH sorbent.

Table 2 The evaluated kinetic parameters; Pseudo first order, and pseudo-second order models

Pseudo first-order model	
q_1 (mg g^{-1})	87.0
k_1 (min^{-1})	0.073
χ^2	5.7
R^2	0.98
Pseudo second-order model	
q_2 (mg g^{-1})	94.7
k_2 (min^{-1})	0.0013
h (mol g^{-1} h^{-1})	12.0
$t_{1/2}$ (h)	7.9
χ^2	0.19
R^2	0.99

determining step in the Zr(IV) uptake using Zn/Al-NLDH is chemisorption, and the adsorption process involves the participation of a pair of electrons between the Zr(IV) and the functional groups on the Zn/Al-NLDH surface.[33–36] Other studies, such as those on Zr(IV) adsorption from aqueous solution by magnetic cellulose/chitosan nanocomposites,[2] *in situ*-gel-precipitated aluminium-based composite sorbents modified,[3] polyacrylamide titanium tungstosilicate,[6] polyaniline/SiO_2 composite,[16,17] activated charcoal,[26] and clinoptilolite,[32] have also shown similar kinetic performance.

It is possible to understand the process of Zr(IV) adsorption by analyzing the data using Weber–Morris models. Fig. 9, which shows the diversity of sorption capacity against $t^{0.5}$, consists of two line segments that indicate two stages. The statement implies that there are several interaction mechanisms controlling the adsorption process. The terms of the W–M equation can be found in Table S2†. The results show that the adsorption process has different performances at each stage. At the beginning of the adsorption process, the Zn/Al-NLDH has free surface active sites, which results in a high reaction rate (K_i = 10.12 mg g^{-1} min$^{-1/2}$). The high concentration of Zr(IV) ions in the solution enables rapid diffusion of the ions onto the sorbent surface. This results in a low boundary effect (C = 18.1),[35,36] indicating a chemisorption interaction between Zn/Al-NLDH and Zr(IV) that extends to the equilibrium stage. However, at the equilibrium stage, most of the active sites on the sorbent are occupied, leading to a reduced driving force of Zr(IV) and a low rate of reaction (K_i = 0.88 mg g^{-1} min$^{-1/2}$) and a high boundary effect (C = 78.3).[35,36] Therefore, the intra-particular diffusion of Zr(IV) ions into the sorbent pores takes place through a physisorption interaction mechanism.

3.2.3. Isotherm investigation. The adsorption isotherm is an important tool for describing the interaction between adsorbate species and sorbent solid surface active sites. It expresses the relation between the adsorbate concentration in the solid and liquid phases and can help improve the design of adsorption systems.[37–39] To better understand the isotherm demeanor of Zr(IV) adsorption using Zn/Al-NLDH material, a series of trials were run with different initial concentration ranges of 10–80 mg L^{-1}. The trials were conducted under fixed conditions of 120 minutes shaking time, a temperature of 25 ± 1 °C, pH of 2.0, and a 0.5 g L^{-1} sorbent dose. The results, shown in Fig. 10, indicate that the sorbent's affinity to Zr(IV) ions is rapidly boosted with the original concentration increment from 10 to 60 mg L^{-1}. This is likely due to the Zn/Al-NLDH material providing free function groups for interaction with Zr(IV) species.[16–18] However, when the initial concentration is prolonged, the saturation of most surface function groups results in a slower uptake process.[16–18]

The detailed isotherm of Zr(IV) adsorption can be analyzed by using conventional isotherm equations such as Freundlich, Langmuir, Sips, and Temkin models.[37–39] The references used to develop these models are mentioned in the study. The equations used in the models are provided in Table S1†. The fitting of the models is evaluated using the Chi-square (χ^2) and coordination coefficient (R^2) equations mentioned in Table S1.†[35,36] The sorption capacity (q_e) of Zr(IV) is plotted against the residual concentration (isotherm curve) in Fig. 11, while the values of the isotherm variables are provided in Table 3.

Based on the results presented in Table 3, it is observed that the Langmuir isotherm model has the lowest Chi-square

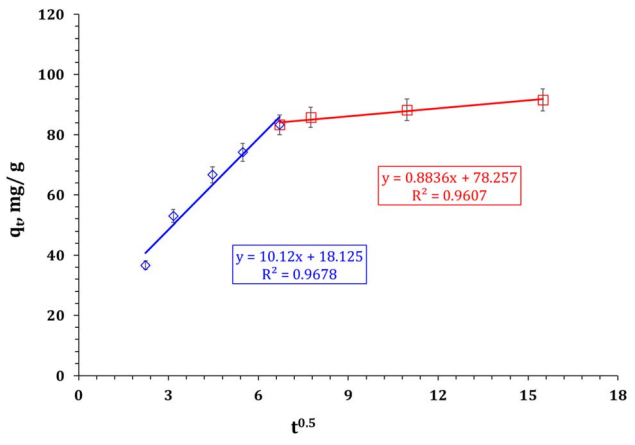

Fig. 9 Morris–Weber model plot for Zr(IV) sorption using Zn/Al-NLDH sorbent.

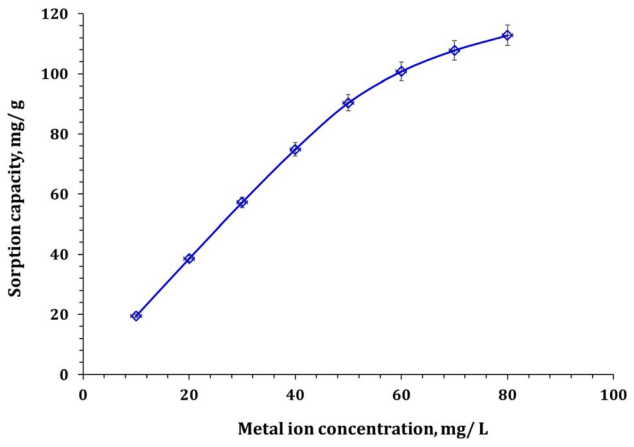

Fig. 10 The effect of Zr(IV) initial concentration on the uptake process (pH 2.0, temperature 25 °C, reaction time of 120 min, sorbent dose of 0.5 g L^{-1}).

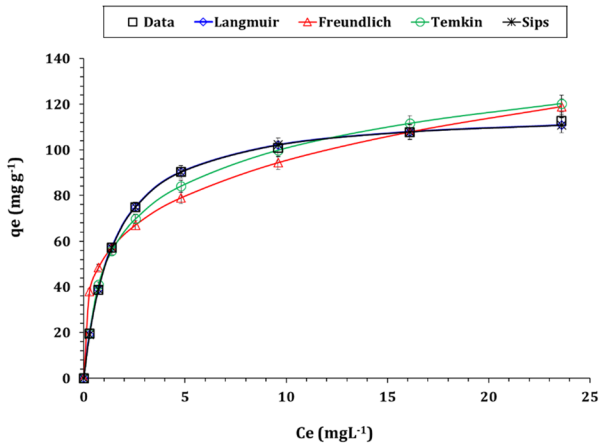

Fig. 11 Isotherm profile for Zr(IV) sorption using Zn/Al-NLDH sorbent.

Table 3 The evaluated variables of Langmuir, Freundlich, Temkin, and Sips isotherm models

Freundlich model		**Langmuir model**	
$1/n_F$	0.3	q_m (mgg^{-1})	117.6
k_F (mg g^{-1}) (mg L^{-1})	52.7	k_L (L mg^{-1})	0.7
χ^2	14.4	χ^2	0.07
R^2	0.93	R^2	0.99
Sips model		**Temkin model**	
q_S (mg g^{-1})	117.7	b_T (J mol^{-1})	108.9
k_S (L mg^{-1})	0.7	A_T (L g^{-1})	8.4
m_S	1.0	χ^2	1.7
χ^2	0.07	R^2	0.98
R^2	0.99		

coefficient of 0.07 and the highest coordination coefficient of 0.99. This indicates that the adsorption nature is uniform and homogeneous.[37–39] The highest capacity (q_m) for Zn/Al-NLDH sorbent towards Zr(IV) ions is approximately 117.7 mg g^{-1}. The process of Zr(IV) adsorption is favorable, which is evident from the dimensionless equilibrium term $R_L = (1/(1 + K_L C_o))$. If the value of R_L is between zero and one, then the process is favorable. On the other hand, if R_L is greater than one, then the process is unfavorable.[37–39] According to the data presented in Fig. S1,† the R_L values were between zero and one, indicating a favorable adsorption process. Similar isotherm performance was observed in various studies such as the adsorption of Zr(IV) from aqueous solution by magnetic cellulose/chitosan nanocomposites,[2] *in situ*-gel-precipitated aluminum-based composite sorbents modified,[3] polyacrylamide titanium tungstosilicate,[6] polyaniline/SiO_2 composite,[16,17] activated charcoal,[31] and clinoptilolite.[32] These studies all demonstrated a monolayer, uniform, and homogeneous adsorption process.

The Sips isotherm model combines the Freundlich and Langmuir models to predict the adsorption process. It is useful for heterogeneous adsorption at low adsorbate concentrations and reduces to the Langmuir isotherm model at high concentrations. The results from Table 3 show that the Sips model fits the experimental results well with a low Chi-square coefficient (χ^2: 0.07) and a high coordination coefficient (R^2: 0.99). As per the Sips model, q_S and q_m values are the same, with a maximum sorption capacity of 117.7 mg g^{-1}. The strong correlation with this model suggests that the adsorption process involves both monolayer coverage (as in the Langmuir model) and heterogeneous surface energies (as accounted for in the Sips model), indicating a complex adsorption mechanism.[37–39]

The Freundlich isotherm model has a coordination coefficient ($R^2 = 0.93$), indicating that the Zn/Al-NLDH sorbent can effectively uptake Zr(IV) even at low initial concentrations. It suggests that the Zr(IV) uptake process is predominantly a monolayer process, with a slight contribution from the multilayer adsorption process.[37–39] The adsorption intensity ratio, $1/n_F$, can be used to determine the profile of the Zr(IV) adsorption process. If $1/n_F$ is less than one, the process is favorable, and if it is greater than one, the process is unfavorable.[37–39] The data in Table 3 shows that $1/n_F$ is 0.3, indicating the favorability of the Zr(IV) uptake process.

The Temkin model assumes a uniform and ideal surface with uniform distribution and energy for each adsorption site. The anticipated data declares that the Temkin isotherm model exhibits a good coordination coefficient (0.98), confirming a uniform and ideal adsorbent surface which is consistent with the findings of the Langmuir isotherm model. The magnitude of the heat of adsorption (b_T) value (108.9 J mol^{-1}) is less than 8 kJ mol^{-1}, elucidating a physisorption nature for the Zr(IV) adsorption process.[37–39] Finally, the inferences from isotherm studies are consistent with the outcomes from the W–M kinetic model whereas the adsorption of Zr(IV) ions is controlled by multiple reaction mechanisms.

Table 4 shows the sorption capacity of Zn/Al-NLDH sorbent for Zr(IV) ions, with a comparison to other sorbents in the literature. The results show that the prepared sorbent has an appropriate sorption capacity.

3.2.4. Impact of sorbent dosage. It is commonly known that the amount of sorbent added is a crucial variable for optimizing the sorbent dosage and economic assessment of the proposed process. To determine the dependence of Zn/Al-NLDH sorbent capacity on the sorbent dosage, several experiments

Table 4 Comparison of sorption performance of Zr(IV) for different sorbents

Sorbent	pH	Adsorption capacity mg g^{-1}	References
MCCh-N	1.8	180.0	2
MCCh-8H	2	168.0	
Dowex 50WX8 50	—	172.4	7
Amberlite	—	149.6	
PGMS	2.6	72.2	40
SGMS		45.0	
SGN18	3	38.4	41
PGMS	2.6	72.2	42
SGMS	2.6	45.0	
MPFSG	1.8	12.3	43
BPFSG		16.7	
AAPPFSG		29.2	
Zn/Al-NLDH	2	117.6	This work

were conducted at a Zn/Al-NLDH dose of 0.2–0.6 g L^{-1}. The other variables were kept constant at a shaking time of 120 minutes, room temperature, 50 mg L^{-1} original concentration, and a pH of 2.0. Fig. 12 indicates that the Zn/Al-NLDH affinity decreased from 103.1 to 80.6 mg g^{-1} as the sorbent dose increased from 0.2 to 0.6. This could be because the availability of Zn/Al-NLDH surface function groups was higher than that of the existing Zr(IV) ions.[2,3,6,7] It is worth noting that the sorption efficiency increased from 40.1 to 91.7% as the sorbent dose varied from 0.2 to 0.5 g L^{-1}, which was due to the increase in sorbent surface area (more available active sites for binding with Zr(IV) ions).[2,3,6,7]

3.2.5. Thermodynamics investigation. For upscaling the process of adsorption systems, it is important to understand their thermodynamic performance and associated terms. To achieve this, a series of tests were conducted at different reaction temperatures ranging from 25–50 ± 1 °C, while keeping the other parameters constant at 120 minutes of shaking time, 0.5 g L^{-1} of Zn/Al-NLDH dosage, 50 mg L^{-1} original concentration, and solution pH of 2.0. The graph in Fig. 13-I shows the sorption capacity variation with temperature, indicating that the Zr(IV) adsorption process is endothermic. As the reaction temperature increased from 25 to 50 °C, the sorption capacity increased from 90 to 96.2 mg g^{-1}.[35,36] The experimental results were analyzed mathematically using thermodynamic equations (Table S1†) and the Van't Hoff plot (Fig. 13-II) to determine the values of $\Delta S°$ (standard entropy change), $\Delta G°$ (standard Gibbs free energy change), and $\Delta H°$ (standard enthalpy change).[44,45]

The sorption process is endothermic, as indicated by the positive value of the standard enthalpy change ($\Delta H°$ = 34.1 kJ mol^{-1}: Table 5).[44,45] A physical mechanism (physisorption) causing the sorption process is indicated by $\Delta H°$ < 84 kJ mol^{-1}. This finding is also supported by the Temkin isotherm model analysis. The spontaneous nature and feasibility of the Zr(IV) adsorption process is elucidated by the negative value of the standard Gibbs Free energy change.[44,45] The sorption process is more favorable at higher temperatures, as deduced from the change of $\Delta G°$ values from −24.3 to −29.1 kJ mol^{-1} as the temperature increased from 25 to 50 °C.[44,45] However, the Zn/Al-NLDH sorbent's application for Zr(IV) adsorption is considered an energy-efficient process as about 90% sorption efficiency could be achieved at room temperature. Table 5 shows that the adsorption process has a positive entropy change ($\Delta S° = 195.8$ J mol^{-1} K^{-1}). This means that the process is spontaneous, but it is characterized by a positive entropy change. When the adsorbate binds to the surface of the sorbent, it creates more space for other solution components to move around, which increases the system's entropy change.[44,45] This same thermodynamic behavior (*i.e.* endothermic, feasible, and spontaneous) is also observed for the adsorption of Zr(IV) by polyacrylamide titanium tungstosilicate,[6] polyaniline/SiO_2 composite,[16,17] activated charcoal,[31] and clinoptilolite.[32]

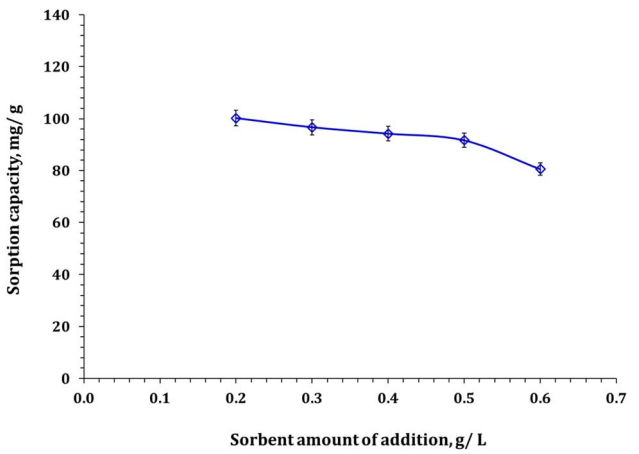

Fig. 12 The effect of Zn/Al-NLDH dose on Zr(IV) uptake (room temperature; 50 mg L^{-1} original concentration; 240 min contact time; pH 2.0).

3.2.6. Impact of interfering ions. Several experiments were conducted to study the effect of a complex matrix on the adsorption capacity of Zr(IV) using Zn/Al-NLDH material. The testes were conducted using a Zr(IV) standard solution of 50 mg L^{-1} mixed with 50 mg L^{-1} of individual interfering ions, namely Fe(III), Ca(II), Ti(IV), Nb(III), and Y(III). The experimental conditions were kept constant at a shaking time of 120 minutes, room temperature, pH of 2.0, and a sorbent dose of 0.5 g L^{-1}. The data presented in Fig. S2† shows that the presence of Ti(IV), Nb(III), and Y(III) slightly decreased the adsorption efficiency of Zr(IV) from 91.0% to about 85%. However, in the presence of Ca(II) and Fe(III), the sorption percentage dramatically decreased to about 69% and 65%, respectively.

3.2.7. Proposed adsorption mechanism. LDHs can be described as $[M_{1-x}^{2+}M_x^{3+}(OH)_2]^{x+}(A^{n-})_{x/n}\cdot mH_2O$, where M^{2+} is divalent metal, M^{3+} is trivalent metal, A^{n-} represents the interlayer anion of LDHs, and x is the molar ratio of $M^{2+}/(M^{2+} + M^{3+})$.[20,46] The LDHs possess a high potential for heavy metal adsorption from wastewater through various mechanisms owing to their unique physicochemical properties, and particular structures.[47–49] These mechanisms include isomorphic substitution, electrostatic interactions, interlayer chemical precipitation, surface complexation, and ion exchange.[49–53]

Different mechanisms can work simultaneously during the application of LDH materials such as the interlayer anions, molar ratio, and cation type. The type of LDH composite determines the primary mechanism. For instance, Mg/Al-LDH with interlayer CO_3^{2-} favors the sorption of heavy metal cations by chemical precipitation, ion exchange, and electrostatic binding mechanisms.[54] In contrast, the isomorphic substitution mechanism dominates the Cd adsorption using Ca/Al-LDH.[50,51] The uranium removal using the LDH mechanism could be described as the interlayer carbonate co-precipitation and the surface complexation reaction between UO_2^{2+} and OH^-/CO_3^{2-} groups.[55,56] Arsenate uptake using Mg–Fe LDHs and Mg–Al LDHs is attributed to the formation of inner-sphere complexes,[57] while the surface precipitation mechanism controls the phosphate adsorption using LDH.[58] However, Cr^{3+} and Cd^{2+} removal using DTPMP-LDH (D-LDH) composite was achieved through the chelation reaction, electrostatic interaction, and weak vdW potential.[59]

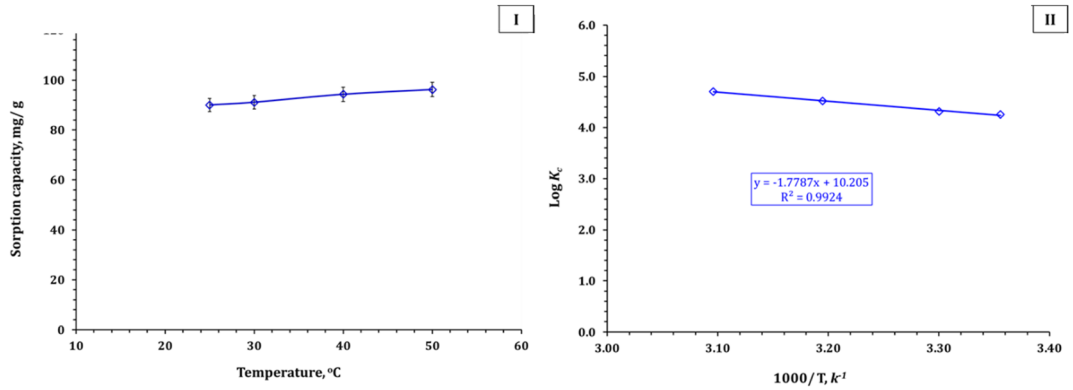

Fig. 13 Effect of sorption temperature on Zr(IV) sorption capacity (I), and Van't Hoff plot for Zr(IV) sorption using Zn/Al-NLDH sorbent (II) (dose 0.5 g L^{-1}, shaking time of 120 min, initial concentration 50 mg L^{-1}, pH 2.0).

Table 5 Thermodynamic parameters for Zr(VI) sorption using Zn/Al-NLDH sorbent

ΔG (kJ mol^{-1})				ΔH	ΔS
25	30	40	50	(kJ mol^{-1})	(J mol^{-1} K^{-1})
−24.3	−25.0	−27.1	−29.1	34.1	195.8

In the present study, the zeta potential analysis declares that the prepared Zn/Al-NLDH sorbent exhibits a negatively charged surface value of −28.9 mV (Fig. 1), while the speciation of Zr(IV) ions over solution pH[2,3,6] displayed a cationic species at the investigated solution pH range, which deduced that the electrostatic interaction between the negative charge of hydroxide layers in NLDH and the positive cation species is contributing the uptake process. This proposal is confirmed by the zeta potential analysis of the Zn/Al-NLDH sorbent after the adsorption process (Fig. 1) whereas, the negativity of the sorbent surface charge is decreased to ≈−19.8 mV after the binding with the positive Zr(IV) cations. The boost of the particle size from ≈140 nm for the Zn/Al-NLDH to 268 nm after the adsorption process (Fig. 1) confirms the outer-sphere complexes between the sorbent surface and the Zr(IV) ions. Furthermore, Zr(IV) species could form inner-sphere complexes with the hydroxyl function group on the surface of the Zn/Al-NLDH sorbent. The surface complexation mechanism is confirmed by the variation of the FTIR analysis for the Zn/Al-NLDH sorbent before and after the uptake process (Fig. 5) whereas, the peak of the –OH group is changed after the adsorption process reflecting the complex formation mechanism. This mechanism is consistent with the findings of the kinetic analysis results which elucidated that the Pseudo-second order kinetic model is the best model for describing the adsorption process which reflects the chemisorption interaction through the inner surface complexation mechanism.

Morris–Weber kinetic model (Fig. 9) reveals that Zr(IV) adsorption using the Zn/Al-NLDH is controlled with multiple reaction mechanisms, and the chemisorption mechanisms such as surface complexation is the main contributor at the beginning of the process, while after the equilibrium stage, the physisorption mechanisms such as the inter-particular diffusion mechanism is mainly contribute the uptake process. This elaboration is confirmed by the decrease in the sorbent surface area from 730.5 to 163.3 cm^2 g^{-1} (Table 1). The physisorption mechanisms is also confirmed with the findings of the thermodynamic and isotherm analysis which declare that the $\Delta H°$ value is 34.1 kJ mol^{-1}, and the b_T value (108.9 J mol^{-1}) which indicates the physisorption process using the weak vdW interaction mechanism.

3.2.8. Investigation of desorption and recycling process. For the successful development and feasibility assessment of the adsorption process, it is crucial to test the prepared materials for their ability to undergo desorption and reusability. In this regard, tests were conducted to explore the loaded Zn/Al-NLDH desorption using various aqueous solutions such as sulfuric, hydrochloric, and nitric acids. The experimental conditions were as follows: an acid concentration of 1.0 M, room temperature, 120 minutes of shaking time, and 0.5 g L^{-1} sorbent dosage. It is evident from Table S3† that the affinity of aqueous solutions for Zr(VI) elution from the loaded sorbent can be ranked as hydrochloric acid > sulfuric acid > nitric acid. The desorption percentage of the applied mineral acid solutions was about 98.1%, 76.7%, and 64.3% for hydrochloric, sulfuric, and nitric acids, respectively. The reusability of the Zn/Al-NLDH material was tested for six consecutive sorption/desorption cycles. Before each cycle, the sorbent was washed with deionized water. The data in Table S4† shows that the Zn/Al-NLDH sorbent demonstrated good stability after six cycles. However, the sorption efficiency decreased from 90.6% to 88.7% and the desorption percentage decreased from 98.0% to 95.8%.

3.2.9. Waste effluent treatment. Effective waste management is crucial for protecting the environment and human health. In this regard, scientists conducted an experiment using a Zn/Al-NLDH material to treat a wastewater sample obtained from the Nuclear Materials Authority in Egypt. The sample's main components were determined using ICP-AES and listed in Table S5†. The experiment was conducted at room temperature and a pH of 2.0, with a shaking time of 120 minutes, and a sorbent dosage of 0.5 g L^{-1}. After the shaking process, the

solid and liquid parts were separated. The results revealed that around 87.5% of Zr(VI) ions were effectively removed from the raffinate solution. It is worth noting that the removal efficiencies for Ti(IV), Fe(III), and V(IV) ions were around 15.2%, 17.4%, and 3.0%, respectively. Moreover, the concentration of Na(I) and K(I) ions was reduced by around 2.8% and 5.2%. These findings indicate that the Zn/Al-NLDH material can be effectively used in hydrometallurgical processes.

4 Conclusion

A nanostructured layered double hydroxide (Zn/Al-NLDH) composed of zinc and aluminum has been successfully created and utilized to eliminate Zr(IV) from an aqueous solution. The sorbent's textural properties, and structure were examined using SEM, EDX, BET-surface area, and XRD. The study comprehensively investigated the primary parameters that influence the adsorption process, such as pH, shaking time, reaction temperature, sorbent dose, and original concentration. Pseudo second order kinetic model and Langmuir isotherm model were recognized to be well fit the experimental data of Zr(IV) uptake. The highest uptake affinity of the Zn/Al-NLDH sorbent for Zr(IV) ions was about 117.6 mg g^{-1}. The findings of the thermodynamic analysis elucidated an endothermic, feasible, and spontaneous uptake process. Furthermore, 1.0 M hydrochloric acid was effectively used to achieve around 96% of Zr(VI) adsorption from the loaded sorbent, and the Zn/Al-NLDH sorbent remained stable for six consecutive sorption/desorption cycles. Overall, the results showed that the synthesized Zn/Al-NLDH sorbent is an appropriate material for the wastewater remediation process.

Consent to participate

All of the authors consented to participate in the drafting of this manuscript.

Data availability

All the data used for this work are publicly available.

Author contribution

All authors contributed to the study conception and design, material preparation, data collection and analysis. All authors read and approved the final manuscript.

Conflicts of interest

The authors of this manuscript have no competing or conflict of interest with any person or any organization.

Acknowledgements

The authors received no financial support for the research, authorship, and/or publication of this article.

References

1 M. Wu, H. He, F. Xu, Z. Xu, W. Zhang, Z. He, J. Qu, R. Chi and L. Huang, High-efficient and selective extraction of Hf over Zr with DIBK-P350 synergistic extraction system, *Sep. Purif. Technol.*, 2019, **212**, 255–261, DOI: 10.1016/J.SEPPUR.2018.11.043.

2 A. E. Mubark, Sequestration of zirconium and hafnium content using magnetic cellulose/chitosan nanocomposites from waste effluents, *J. Water Process Eng.*, 2024, **58**, 104759, DOI: 10.1016/J.JWPE.2023.104759.

3 M. S. Hagag, A. E. Mubark, A. A. Eliwa and A. M. Abdel-Razik, Retrieval of zirconium ions from laboratory solutions upon *in situ*-gel-precipitated aluminium based composite sorbents, *Colloids Surf., A*, 2024, **682**, 132921, DOI: 10.1016/J.COLSURFA.2023.132921.

4 H. H. El Agamy, A. E. Mubark, E. A. Gamil, N. A. Abdel-Fattah and A. A. Eliwa, Preparation of zirconium oxide nanoparticles from rosette concentrate using two distinct and sequential techniques: hydrothermal and fusion digestion, *Chem. Pap.*, 2023, **77**, 3229–3240, DOI: 10.1007/S11696-023-02699-2/FIGURES/9.

5 A. H. El-Afandy, A. M. Yousif and A. E. Mubark, Subsequent Separation of Niobium (Nb), Thorium (Th), Rare Earth Elements (REEs), Zirconium (Zr), and Uranium (U) from Abu Rusheid Cataclastic Concentrate, South Eastern Desert, Egypt, *Radiochemistry*, 2022, **64**, 257–267, DOI: 10.1134/S1066362222020175/FIGURES/8.

6 M. F. Hamza, A. Gamal, G. Hussein, M. S. Nagar, A. A. H. Abdel-Rahman, Y. Wei and E. Guibal, Uranium(VI) and zirconium(IV) sorption on magnetic chitosan derivatives – effect of different functional groups on separation properties, *J. Chem. Technol. Biotechnol.*, 2019, **94**, 3866–3882, DOI: 10.1002/JCTB.6185.

7 E. C. B. Felipe and A. C. Q. Ladeira, Separation of zirconium from hafnium by ion exchange, *Sep. Sci. Technol.*, 2018, **53**, 330–336, DOI: 10.1080/01496395.2017.1385624.

8 Y. Ma, S. Stopic, Z. Huang and B. Friedrich, Selective recovery and separation of Zr and Hf from sulfuric acid leach solution using anion exchange resin, *Hydrometallurgy*, 2019, **189**, 105143, DOI: 10.1016/J.HYDROMET.2019.105143.

9 L. Y. Wang and M. S. Lee, A review on the aqueous chemistry of Zr(IV) and Hf(IV) and their separation by solvent extraction, *J. Ind. Eng. Chem.*, 2016, **39**, 1–9, DOI: 10.1016/J.JIEC.2016.06.004.

10 A. B. Botelho Junior, D. C. R. Espinosa and J. A. S. Tenório, Selective separation of Sc(III) and Zr(IV) from the leaching of bauxite residue using trialkylphosphine acids, tertiary amine, tri-butyl phosphate and their mixtures, *Sep. Purif. Technol.*, 2021, **279**, 119798, DOI: 10.1016/J.SEPPUR.2021.119798.

11 D. J. Branken, G. Lachmann, H. M. Krieg and D. S. L. Bruinsma, Influence of KF and HF on the Selectivity of Zr and Hf Separation by Fractional Crystallization of K2Zr(Hf)F6, *Ind. Eng. Chem. Res.*, 2010,

49, 797–808, DOI: 10.1021/IE900747K/SUPPL_FILE/IE900747K_SI_001.PDF.

12 Y. Ma, S. Stopic, X. Wang, K. Forsberg and B. Friedrich, Basic Sulfate Precipitation of Zirconium from Sulfuric Acid Leach Solution, *Metals*, 2020, **10**, 1099, DOI: 10.3390/MET10081099.

13 H. E. Rizk, A. M. S. El-Din, E. M. E. Afifi and M. F. Attallah, Potential separation of zirconium and some lanthanides of the nuclear and industrial interest from zircon mineral using cation exchanger resin, *J. Dispersion Sci. Technol.*, 2022, **43**, 1642–1651, DOI: 10.1080/01932691.2021.1878039.

14 L. Poriel, S. Pellet-Rostaing, V. Lamotte, M. Lemaire and A. Favre-Réguillon, Zirconium and Hafnium Separation, Part 2. Solid/Liquid Extraction in Hydrochloric Acid Aqueous Solution with Anion Exchange Resins, *Sep. Sci. Technol.*, 2006, **41**, 2711–2722, DOI: 10.1080/01496390600725711.

15 M. Smolik, A. Jakóbik-Kolon and M. Porański, Separation of zirconium and hafnium using Diphonix® chelating ion-exchange resin, *Hydrometallurgy*, 2009, **95**, 350–353, DOI: 10.1016/J.HYDROMET.2008.05.010.

16 E. A. Abdel-Galil, A. S. Tourky and A. E. Kasem, Sorption of some radionuclides from nuclear waste effluents by polyaniline/SiO2 composite: Characterization, thermal stability, and gamma irradiation studies, *Appl. Radiat. Isot.*, 2020, **156**, 109009, DOI: 10.1016/J.APRADISO.2019.109009.

17 A. E. Kasem, E. A. Abdel-Galil, N. Belacy and N. A. Badawy, Kinetics and adsorption equilibrium of some radionuclides on polyaniline/SiO2composite, *Radiochim. Acta*, 2021, **109**, 85–97, DOI: 10.1515/RACT-2020-0014/MACHINEREADABLECITATION/RIS.

18 A. S. Suneesh, B. R. Selvan and N. Ramanathan, A chemically functionalized hydroxyacetamide anchored polymeric adsorbent for the selective separation of zirconium from acidic aqueous solutions, *React. Funct. Polym.*, 2022, **172**, 105173, DOI: 10.1016/J.REACTFUNCTPOLYM.2022.105173.

19 L. Xu, Y. Xiao, A. van Sandwijk, Q. Xu and Y. Yang, Separation of Zirconium and Hafnium: A Review, *Energy Mater.*, 2014, 451–457, DOI: 10.1007/978-3-319-48765-6_53.

20 A. V. Karim, A. Hassani, P. Eghbali and P. V. Nidheesh, Nanostructured modified layered double hydroxides (LDHs)-based catalysts: A review on synthesis, characterization, and applications in water remediation by advanced oxidation processes, *Curr. Opin. Solid State Mater. Sci.*, 2022, **26**, 100965, DOI: 10.1016/J.COSSMS.2021.100965.

21 R. Pelalak, A. Hassani, Z. Heidari and M. Zhou, State-of-the-art recent applications of layered double hydroxides (LDHs) material in Fenton-based oxidation processes for water and wastewater treatment, *Chem. Eng. J.*, 2023, **474**, 145511, DOI: 10.1016/J.CEJ.2023.145511.

22 Y. Zheng, B. Cheng, W. You, J. Yu and W. Ho, 3D hierarchical graphene oxide-NiFe LDH composite with enhanced adsorption affinity to Congo red, methyl orange and Cr(VI) ions, *J. Hazard. Mater.*, 2019, **369**, 214–225, DOI: 10.1016/J.JHAZMAT.2019.02.013.

23 R. K. Gautam, A. K. Singh and I. Tiwari, Nanoscale layered double hydroxide modified hybrid nanomaterials for wastewater treatment: A review, *J. Mol. Liq.*, 2022, **350**, 118505, DOI: 10.1016/J.MOLLIQ.2022.118505.

24 M. A. Ahmed and A. A. Mohamed, A systematic review of layered double hydroxide-based materials for environmental remediation of heavy metals and dye pollutants, *Inorg. Chem. Commun.*, 2023, **148**, 110325, DOI: 10.1016/J.INOCHE.2022.110325.

25 A. Meawad and S. Ibrahim, Novel bifunctional dispersing agents from waste PET packaging materials and interaction with cement, *Waste Manag.*, 2019, **85**, 563–573, DOI: 10.1016/J.WASMAN.2019.01.028.

26 S. Ibrahim, M. E. El-Naggar, A. M. Youssef and M. S. Abdel-Aziz, Functionalization of Polystyrene Nanocomposite with Excellent Antimicrobial Efficiency for Food Packaging Application, *J. Cluster Sci.*, 2020, **31**, 1371–1382, DOI: 10.1007/S10876-019-01748-9/FIGURES/8.

27 M. M. Abdellatif, F. H. H. Abdellatif and S. Ibrahim, The utilization of cross-linked gelatin/PAMAM aerogels as heavy metal ions bio-adsorbents from aqueous solutions, *Polym. Bull.*, 2022, **79**, 10931–10948, DOI: 10.1007/S00289-021-04019-8/METRICS.

28 L. P. Cardoso, R. Celis, J. Cornejo and J. B. Valim, Layered Double Hydroxides as Supports for the Slow Release of Acid Herbicides, *J. Agric. Food Chem.*, 2006, **54**, 5968–5975, DOI: 10.1021/JF061026Y.

29 H. E. Salman and N. J. Hussein, Synthesis of Zinc-Aluminum Layered Double Hydroxides and Application of Adsorption for Nitrate from Water, *IOP Conf. Ser.: Mater. Sci. Eng.*, 2019, **571**, 012070, DOI: 10.1088/1757-899X/571/1/012070.

30 F. Z. Mahjoubi, A. Khalidi, M. Abdennouri and N. Barka, Zn–Al layered double hydroxides intercalated with carbonate, nitrate, chloride and sulphate ions: Synthesis, characterisation and dye removal properties, *J. Taibah Univ. Sci.*, 2017, **11**, 90–100, DOI: 10.1016/J.JTUSCI.2015.10.007.

31 M. M. Hamed, H. E. Rizk and I. M. Ahmed, Adsorption behavior of zirconium and molybdenum from nitric acid medium using low-cost adsorbent, *J. Mol. Liq.*, 2018, **249**, 361–370, DOI: 10.1016/J.MOLLIQ.2017.11.049.

32 H. Faghihian and M. Kabiri-Tadi, Removal of zirconium from aqueous solution by modified clinoptilolite, *J. Hazard. Mater.*, 2010, **178**, 66–73, DOI: 10.1016/J.JHAZMAT.2010.01.044.

33 Q. Hu, S. Pang and D. Wang, In-depth Insights into Mathematical Characteristics, Selection Criteria and Common Mistakes of Adsorption Kinetic Models: A Critical Review, *Sep. Purif. Rev.*, 2022, **51**, 281–299, DOI: 10.1080/15422119.2021.1922444.

34 C. Yao and T. Chen, A film-diffusion-based adsorption kinetic equation and its application, *Chem. Eng. Res. Des.*, 2017, **119**, 87–92, DOI: 10.1016/J.CHERD.2017.01.004.

35 A. Elzoghby, H. Fahmy, M. Taha and S. Ibrahim, Active carbon-based waste packaging materials for uranium sorption from aqueous solution, *Environ. Sci. Pollut. Res.*,

2023, **30**, 74726–74741, DOI: 10.1007/S11356-023-27269-7/TABLES/7.

36 A. F. Abou-Hadid, U. A. El-Behairy, M. M. Elmalih, E. Amdeha, A. M. A. El Naggar, M. H. Taha and A. E. M. Hussein, Production of efficient carbon fiber from different solid waste residuals for adsorption of hazardous metals from wastewater samples, *Biomass Convers. Biorefin.*, 2022, **1**, 1–16, DOI: 10.1007/S13399-022-03097-6/FIGURES/16.

37 J. Wang and X. Guo, Adsorption isotherm models: Classification, physical meaning, application and solving method, *Chemosphere*, 2020, **258**, 127279, DOI: 10.1016/J.CHEMOSPHERE.2020.127279.

38 M. A. Al-Ghouti and D. A. Da'ana, Guidelines for the use and interpretation of adsorption isotherm models: A review, *J. Hazard. Mater.*, 2020, **393**, 122383, DOI: 10.1016/J.JHAZMAT.2020.122383.

39 M. H. Taha, Sorption of U(VI), Mn (II), Cu(II), Zn(II), and Cd(II) from multi-component phosphoric acid solutions using MARATHON C resin, *Environ. Sci. Pollut. Res.*, 2021, **28**, 12475–12489, DOI: 10.1007/S11356-020-11256-3/TABLES/7.

40 H. Hamedi, S. Moradi, S. M. Hudson and A. E. Tonelli, Chitosan based hydrogels and their applications for drug delivery in wound dressings: A review, *Carbohydr. Polym.*, 2018, **199**, 445–460, DOI: 10.1016/J.CARBPOL.2018.06.114.

41 W. Qin, S. Xu, G. Xu, Q. Xie, C. Wang and Z. Xu, Preparation of silica gel bound crown ether and its extraction performance towards zirconium and hafnium, *Chem. Eng. J.*, 2013, **225**, 528–534, DOI: 10.1016/J.CEJ.2013.03.127.

42 A. M. Donia, A. A. Atia, A. M. Daher, O. A. Desouky and E. A. Elshehy, Extraction and separation of zr(IV) from hydrochloric acid solution using modified silica gel produced from waste solution of sodium silicate, *Sep. Sci. Technol.*, 2011, **46**, 1329–1336, DOI: 10.1080/01496395.2011.558036.

43 A. Das, K. R. S. Chandrakumar, B. Paul, S. M. Chopade, S. Majumdar, A. K. Singh and V. Kain, Enhanced adsorption and separation of zirconium and hafnium under mild conditions by phosphoric acid based ligand functionalized silica gels: Insights from experimental and theoretical investigations, *Sep. Purif. Technol.*, 2020, **239**, 116518, DOI: 10.1016/J.SEPPUR.2020.116518.

44 T. A. Saleh, Kinetic models and thermodynamics of adsorption processes: classification, *Interface Sci. Technol.*, 2022, **34**, 65–97, DOI: 10.1016/B978-0-12-849876-7.00003-8.

45 A. Morsy, M. H. Taha, M. Saeed, A. Waseem, M. A. Riaz and M. M. Elmaadawy, Isothermal, kinetic, and thermodynamic studies for solid-phase extraction of uranium (VI) *via* hydrazine-impregnated carbon-based material as efficient adsorbent, *Nucl. Sci. Tech.*, 2019, **30**, 1–11, DOI: 10.1007/S41365-019-0686-Z/TABLES/5.

46 X. Guan, X. Yuan, Y. Zhao, H. Wang, H. Wang, J. Bai and Y. Li, Application of functionalized layered double hydroxides for heavy metal removal: A review, *Sci. Total Environ.*, 2022, **838**, 155693, DOI: 10.1016/J.SCITOTENV.2022.155693.

47 Z. Tang, Z. Qiu, S. Lu and X. Shi, Functionalized layered double hydroxide applied to heavy metal ions absorption: A review, *Nanotechnol. Rev.*, 2020, **9**, 800–819, DOI: 10.1515/NTREV-2020-0065/ASSET/GRAPHIC/J_NTREV-2020-0065_FIG_006.JPG.

48 S. Zhao, Z. Meng, X. Fan, R. Jing, J. Yang, Y. Shao, X. Liu, M. Wu, Q. Zhang and A. Liu, Removal of heavy metals from soil by vermiculite supported layered double hydroxides with three-dimensional hierarchical structure, *Chem. Eng. J.*, 2020, **390**, 124554, DOI: 10.1016/J.CEJ.2020.124554.

49 X. J. Zhao, S. M. Xu, P. Yin, J. Y. Guo, W. Zhang, Y. Jie and H. Yan, Theoretical study on the mechanism of super-stable mineralization of LDHs in soil remediation, *Chem. Eng. J.*, 2023, **451**, 138500, DOI: 10.1016/J.CEJ.2022.138500.

50 X. Kong, R. Ge, T. Liu, S. Xu, P. Hao, X. Zhao, Z. Li, X. Lei and H. Duan, Super-stable mineralization of cadmium by calcium-aluminum layered double hydroxide and its large-scale application in agriculture soil remediation, *Chem. Eng. J.*, 2021, **407**, 127178, DOI: 10.1016/J.CEJ.2020.127178.

51 B. Zeng, Q. Wang, L. Mo, F. Jin, J. Zhu and M. Tang, Synthesis of Mg-Al LDH and its calcined form with natural materials for efficient Cr(VI) removal, *J. Environ. Chem. Eng.*, 2022, **10**, 108605, DOI: 10.1016/J.JECE.2022.108605.

52 D. Fu, T. A. Kurniawan, R. Avtar, P. Xu and M. H. D. Othman, Recovering heavy metals from electroplating wastewater and their conversion into Zn2Cr-layered double hydroxide (LDH) for pyrophosphate removal from industrial wastewater, *Chemosphere*, 2021, **271**, 129861, DOI: 10.1016/J.CHEMOSPHERE.2021.129861.

53 Q. Sun, C. Liu, P. Cui, T. Fan, M. Zhu, M. E. Alves, M. G. Siebecker, D. L. Sparks, T. Wu, W. Li, D. Zhou and Y. Wang, Formation of Cd precipitates on γ-Al_2O_3: Implications for Cd sequestration in the environment, *Environ. Int.*, 2019, **126**, 234–241, DOI: 10.1016/J.ENVINT.2019.02.036.

54 R. ran Shan, L. guo Yan, K. Yang, Y. feng Hao and B. Du, Adsorption of Cd(II) by Mg–Al–CO3- and magnetic Fe3O4/Mg–Al–CO3-layered double hydroxides: Kinetic, isothermal, thermodynamic and mechanistic studies, *J. Hazard. Mater.*, 2015, **299**, 42–49, DOI: 10.1016/J.JHAZMAT.2015.06.003.

55 X. Guo, Y. Ruan, Z. Diao, K. Shih, M. Su, G. Song, D. Chen, S. Wang and L. Kong, Environmental-friendly preparation of Ni–Co layered double hydroxide (LDH) hierarchical nanoarrays for efficient removing uranium (VI), *J. Clean. Prod.*, 2021, **308**, 127384, DOI: 10.1016/J.JCLEPRO.2021.127384.

56 Y. Guo, Z. Gong, C. Li, B. Gao, P. Li, X. Wang, B. Zhang and X. Li, Efficient removal of uranium (VI) by 3D hierarchical Mg/Fe-LDH supported nanoscale hydroxyapatite: A synthetic experimental and mechanism studies, *Chem. Eng. J.*, 2020, **392**, 123682, DOI: 10.1016/J.CEJ.2019.123682.

57 M. Yoshida, P. Koilraj, X. Qiu, T. Hirajima and K. Sasaki, Sorption of arsenate on MgAl and MgFe layered double hydroxides derived from calcined dolomite, *J. Environ. Chem. Eng.*, 2015, **3**, 1614–1621, DOI: 10.1016/J.JECE.2015.05.016.

58 P. Koilraj and S. Kannan, Phosphate uptake behavior of ZnAlZr ternary layered double hydroxides through surface precipitation, *J. Colloid Interface Sci.*, 2010, **341**, 289–297, DOI: **10.1016/J.JCIS.2009.09.059**.

59 S. Zhu, M. A. Khan, T. Kameda, H. Xu, F. Wang, M. Xia and T. Yoshioka, New insights into the capture performance and mechanism of hazardous metals Cr3+ and Cd2+ onto an effective layered double hydroxide based material, *J. Hazard. Mater.*, 2022, **426**, 128062, DOI: **10.1016/J.JHAZMAT.2021.128062**.